Geophysical Research Letters

RESEARCH LETTER
10.1029/2019GL084199

Global-Scale Observations of the Equatorial Ionization Anomaly

R. W. Eastes[1], S. C. Solomon[2], R. E. Daniell[3], D. N. Anderson[4], A. G. Burns[2], S. L. England[5], C. R. Martinis[6], and W. E. McClintock[1]

[1]Laboratory for Atmospheric and Space Physics, University of Colorado Boulder, Boulder, CO, USA, [2]High Altitude Observatory, National Center for Atmospheric Research, Boulder, CO, USA, [3]Ionospheric Physics, Stoughton, MA, USA, [4]NOAA-SEC and CIRES, University of Colorado Boulder, Boulder, CO, USA, [5]Aerospace and Ocean Engineering, Virginia Polytechnic Institute and State University, Blacksburg, VA, USA, [6]Center for Space Physics, Boston University, Boston, MA, USA

Key Points:
- During geomagnetically quiet solar minimum conditions, significant temporal and spatial variability is observed in the equatorial ionosphere
- At solar minimum, depleted ionospheric regions are observed on most nights, at varying longitudes, and with evident meridional symmetry
- Synoptic-scale disruptions of the ionization crests are seen on several nights, possibly associated with large-scale plasma instabilities

Correspondence to:
R. W. Eastes,
richard.eastes@lasp.colorado.edu

Citation:
Eastes, R. W., Solomon, S. C., Daniell, R. E., Anderson, D. N., Burns, A. G., England, S. L., et al. (2019). Global-scale observations of the equatorial ionization anomaly. *Geophysical Research Letters*, *46*, 9318–9326. https://doi.org/10.1029/2019GL084199

Received 20 JUN 2019
Accepted 3 AUG 2019
Accepted article online 7 AUG 2019
Published online 19 AUG 2019

Abstract The National Aeronautics and Space Administration Global-scale Observations of the Limb and Disk ultraviolet spectrograph has been imaging the equatorial ionization anomaly (EIA), regions of the ionosphere with enhanced electron density north and south of the magnetic equator, since October 2018. The initial 3 months of observations was during solar minimum conditions, and they included observations in December solstice of unanticipated variability and depleted regions. Depletions are seen on most nights, in contrast to expectations from previous space-based observations. The variety of scales and morphologies also pose challenges to understanding of the EIA. Abrupt changes in the EIA location, which could be related to in situ measurements of large-scale depletion regions, are observed on some nights. Such synoptic-scale disruptions have not been previously identified.

Plain Language Summary In this study, ultraviolet images of emissions from the Earth's nighttime ionosphere were examined to determine the location of the equatorial ionization anomaly, regions of enhanced ionization that result in bands of nighttime airglow emission that typically appear parallel to the magnetic equator near +15° and −15° magnetic latitude. We found that gaps in the anomaly are observed much more frequently in these observations than in previous space-based observations. These gaps, sometimes referred to as ionospheric bubbles or depletions, are important because they are associated with ionospheric changes that can cause disruptions in communications and satellite navigation that depend on satellites, such as GPS. The location of the anomaly was also observed to vary significantly, by as much as 15°, from the typical latitudes. The observed level of variability seen during the unusually quiet geomagnetic conditions during which the observations occurred suggests that accurate predictions of the location and variability of the equatorial ionization anomaly requires significant advances in understanding the causes of this variability.

1. Introduction

Two phenomena in the low- and middle-latitude ionosphere—the equatorial ionization anomaly (EIA) and the irregularities that occur within them—have been the subject of decades of research, because they are a critical aspect of ionospheric variability, and have significant effects on communications and navigation systems. Still, they are not understood sufficiently for reliable forecasting of their occurrence.

The EIA (Appleton, 1946) is a result of an eastward electric field along the magnetic equator during the day. Around the magnetic equator, an upward ($\mathbf{E} \times \mathbf{B}$) drift of the ionospheric plasma is produced. Simultaneously, gravity pulls the plasma poleward and downward along the magnetic field lines. As a result of the upward and poleward drift of the plasma, sometimes referred to as a "fountain effect," the nighttime ionospheric *F* region (~200- to 500-km altitude) higher ion and electron densities are seen in two bands near the equator, each typically centered near ±15° magnetic latitude during geomagnetically quiet conditions. Although the production of ions effectively ceases at sunset, the EIA continues to be prominent in the early evening and varies greatly during the night. Recombination of the ions and electrons produces photons, including the 135.6-nm emission observed by the Global-scale Observations of the Limb and Disk (GOLD) imager, but the recombination rates are sufficiently slow that the regions of enhanced ion density may persist through the night.

Variations in electric fields and neutral winds cause changes in the locations and intensities of the two crests of the EIA. The most dramatic changes in the EIA occur shortly after sunset, when the prereversal enhancement (PRE) increases plasma drift velocities. Due to the tilt, offset, and distortion of the Earth's magnetic field and atmospheric tides (e.g., Immel et al., 2006; Lühr et al., 2007), the EIA has additional dependences on geographic location and seasonal change. In addition, during magnetic storms penetration electric fields and neutral wind disturbances of the low-latitude dynamo can disrupt the usual morphology. See Abdu and Kherani (2011) for a more detailed descriptions of the effects of winds on electric fields and ion drifts.

Localized regions in the EIA sometimes become unstable at night, particularly in the early evening, when only the high-altitude *F* region ionosphere persists. This results in microscale and mesoscale density variations whose signatures can be seen in radio, optical, and in situ measurements. This phenomenon is referred to by various names, depending on the observational method: ionospheric irregularities, instabilities, or scintillations; equatorial spread *F*; small-scale plasma depletions; or, more colloquially, "plasma bubbles." Our working hypothesis is that these are all aspects of the same basic process, a result of Rayleigh-Taylor instabilities (Kelley et al., 1976). Radio waves, including those used for communications and Global Navigation Satellite Systems positioning, are disrupted when they encounter the small-scale variations of plasma density that occur at the edges of the depletions. Consequently, the occurrence of ionospheric irregularities are a critical challenge for efforts to predict space weather in the ionosphere. The climatology has been studied using previous satellite observations (e.g., Burke et al., 2004, Burke et al., 2004; Su et al., 2006; Comberiate & Paxton, 2010; Zhan et al., 2018; Rodríguez-Zuluaga et al., 2019), and high-resolution numerical models have succeeded in generating consistent ionospheric structures (e.g., Huba et al., 2008; Retterer, 2010). The observational history of the phenomenon and recent efforts to understand its causation have been reviewed by, for example, Kelly et al. (2011) and Balan et al. (2018).

A primary research objective of the National Aeronautics and Space Administration GOLD mission is to better understand the behavior of the EIA and the instabilities within it. Other objectives and details about them have been discussed by Eastes et al. (2017). The GOLD imager is hosted on the SES-14 communications satellite. Launched in 2018, the satellite is positioned over the equator in a geostationary orbit at 47.5°W longitude, and it measures the Earth's far ultraviolet airglow from ~120°W to ~20°E longitude. The synoptic perspective available from geostationary orbit, combined with the rapid imaging cadence that can be achieved, provides new information that has not been available in previous observations of the EIA. In addition, since the observations can cover longitudes where the geomagnetic equator is north of the geographic equator, as well as longitudes where it is at southern geographic latitudes, the imager is well located for studying the effects of seasonal changes in the neutral atmosphere on equatorial ionosphere. The orbit of the instrument also makes it more feasible to study how changes that occur during the day, prior to sunset, affect the EIA. This paper concentrates on the nightside observations, where rapid changes and depletions occur in the EIA.

2. Observations of the Ultraviolet Nightglow

GOLD images the Earth's sunlit and nightside disk, performs limb scans, and observes stellar occultations, from ~6:00 to ~24:00 universal time each day, avoiding the period when the Sun is too close to the instrument field of view for detector safety. The instrument, which has been described by Eastes et al. (2017) and McClintock et al. (2017), is a spectral imager, with two identical channels observing the 133- to 163-nm wavelength range. Each channel provides spectral information at spatial locations along the entrance slit for either the Northern Hemisphere or the Southern Hemisphere; a 3-D spatial-spectral image "cube" is constructed by scanning from east to west. The independent channels each have a scan mirror, interchangeable slits, and can observe either hemisphere with a 15-min cadence. When only Channel B is in night mode (20:10 to 23:10 UT), imaging alternates between the Northern and Southern Hemispheres. When both channels are in night mode (23:10 to 00:10 UT), Channel A scans the Northern Hemisphere, while Channel B scans the Southern Hemisphere. The medium-resolution slit was used, providing ~0.3-nm spectral resolution. Observations were made at a constant angular resolution that corresponds to ~93-km spatial resolution in the E-W and N-S directions for near nadir observations. In images from GOLD the EIA appears as two bands of 135.6-nm emission on either side of the magnetic equator at night, an example of which is shown in Figure 1.

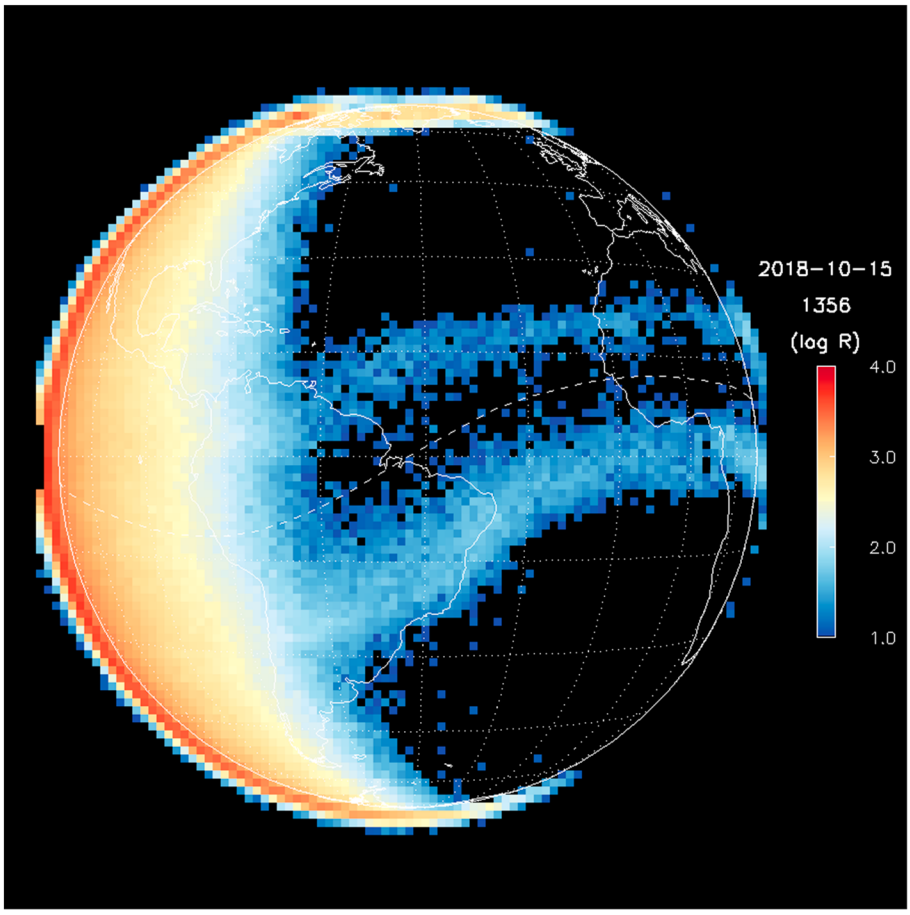

Figure 1. Global-scale Observations of the Limb and Disk image of the daytime airglow and the equatorial ionization anomaly: The image shows the 135.6-nm emission of atomic oxygen on 15 October 2018. The data are from a 24-min scan began at 22:10 UT (19:00 at the subsatellite location, on the equator at 47.5°W longitude). Continental outlines, a 15° latitude-longitude grid, and the location of the magnetic equator have been added to the image. A logarithmic scale is used in order to show the faint nighttime and twilight emissions. The left side of the Earth is sunlit, but the Sun has already set over most of South America, and the transition from day to night is near the East Coast of North America. The equatorial ionization anomaly appears as two arcs on either side of the magnetic equator, extending across the nightside. The aurora can be seen on the horizon at the top and bottom of the Earth.

The ion composition of the *F* region above ~200 km is dominated by atomic oxygen ions, O^+, which can recombine directly with electrons and shed the excess energy by emitting a photon. This *radiative recombination* is slow and the ion densities are low; consequently, the emissions produced are weak, including the 135.6-nm doublet observed by GOLD. The 135.6-nm emission is observed in all modes, and when the component produced by photoelectrons during the daytime fades, the recombination component is prominent. Since the emission is proportional to the square of the ionospheric plasma density, the brightness is indicative of the peak plasma density N_{max}. In this first report, we use column brightness as directly measured by the instrument.

The climatology of the nightside EIA, as observed from the ground and from space, depends on geomagnetic activity and thermospheric neutral winds. However, there is additional night-to-night variability that is driven by other changes, such as those seen in the neutral atmosphere (e.g., Goncharenko et al., 2010; Immel et al., 2009). Earlier observations (e.g., Liu et al., 2007; Luan et al., 2015) have provided climatological descriptions, but higher cadence, synoptic views have rarely been available. The IMAGE mission was able to capture broader morphology when its apogee was at low latitude, but only in the Northern Hemisphere (Immel et al., 2006). Ground-based observations can provide high temporal coverage, but their spatial

coverage is physically limited. The GOLD mission, observing the same longitudes repeatedly and on every night, can provide synoptic measurements of large sections of the EIA. The magnetic equator crosses the geographic equator near the subsatellite point, resulting in longitudinal differences in the orientation of the magnetic field to the geographic coordinate system and hence to the neutral winds (e.g., Anderson & Araujo-Pradere, 2010; Fang et al., 2012; Hagan et al., 2007; Yamazaki & Maute, 2017). This difference in equator location and the simultaneous GOLD observations may help advance comprehension of the EIA.

3. Results and Discussion

3.1. Depletions in the EIA

While the EIA in Figure 1 appears relatively smooth, the night mode observations from late 2018 show that often it is not. An example is shown in Figure 2. On the equatorward edges of the EIA the depletions appear as indentations; the absence of emission from these areas is indicative of depletions in the plasma, produced by instabilities that form and rise through the crests, expanding to higher magnetic latitudes as they grow. The depletions have notable symmetry about the magnetic equator, along field lines extending to the north and south. Understanding the processes responsible for these depletions and predicting their occurrence challenges current modeling and measurement capabilities. Although there are known seasonal and longitudinal dependencies (e.g., Huang, 2017) and a clear association with the strength of the PRE of the equatorial electric field, the sporadic nature of their occurrence is unexplained.

During the October–December 2018 period discussed in this paper, GOLD observed some form of depletions on most nights. Figure 2 is an example of a particularly active night (17 October 2018), with extensive, quasiperiodic, depletions. Comparison of sequential images shows that the depleted regions in Figure 2 moved eastward at ~100 m/s, which is consistent with previous observations (e.g., Balan et al., 2018). Although the depletions may drift by approximately one spatial resolution element during 15 min, the imaging cadence of GOLD, averages can be derived using multiple images. Tracking individual depletions is achievable because the signal levels differ significantly between the depletions and the EIA (background), and the distinctive spatial distributions in the data are readily identifiable. Ground-based imaging, which is available at higher spatial resolution, observes 50- to 300-km depletions that tend to appear in groups separated by ~500 km (Makela et al., 2010; Chapagain et al., 2011; Makela & Otsuka, 2012; Hickey et al., 2018). Consequently, groups of the depletions may sometimes be observed by GOLD as one.

One interesting aspect of the GOLD observations is that they frequently show depletions with uniform spacing, as seen in Figure 2. Depletions with apparently uniform spacing extend across more than 60° of longitude. While the appearance of uniform spacing over such extended longitudes is not ubiquitous, it is frequent. In the 3 months of observations considered, uniform spacing of 3 or more depletions was identifiable on approximately one third of the nights (~34 of 88). The spacing of the depletions varies from day to day, and while the occurrence of uniform spacing could be coincidental, it occurs with sufficient frequency to suggest that a periodic seeding mechanism may be responsible. While possible seeding by gravity waves has been suggested (Earle & Kelley, 1987; Hines, 1960; Tsunoda, 2006), supporting evidence has been limited, and $\mathbf{E} \times \mathbf{B}$ variations consistent with gravity waves have been detected (e.g., Balachandran Nair et al., 1992), uniform spacing has been reported from ground-based imaging (Makela et al., 2010; Takahashi et al., 2015) and possibly by ionosonde (Saito & Maruyama, 2007). In the observations by GOLD most instances of even spacing appear to be of limited duration, with only half spanning beyond one hour of local time (15° of longitude).

3.2. Occurrence Rates of Depletions

The occurrence rates for depletions observed in the GOLD nighttime observations conducted between 1 October and 31 December 2018 are summarized in Table 1. The rates are simple percentages, the number of days on which depletions were identified in a sector divided by the total number of days. The criteria for identification were the presence of either similar structure observable on the equatorward sides of the EIA at magnetic conjugate locations, even if it did not extend through the EIA, or a gap extending through the EIA on one side of the equator.

The occurrences rates were calculated for three longitude regions, each similar to those employed by Burke, Huang, et al. (2004). Viewing conditions are best in the Atlantic region. The view is near vertical, and more

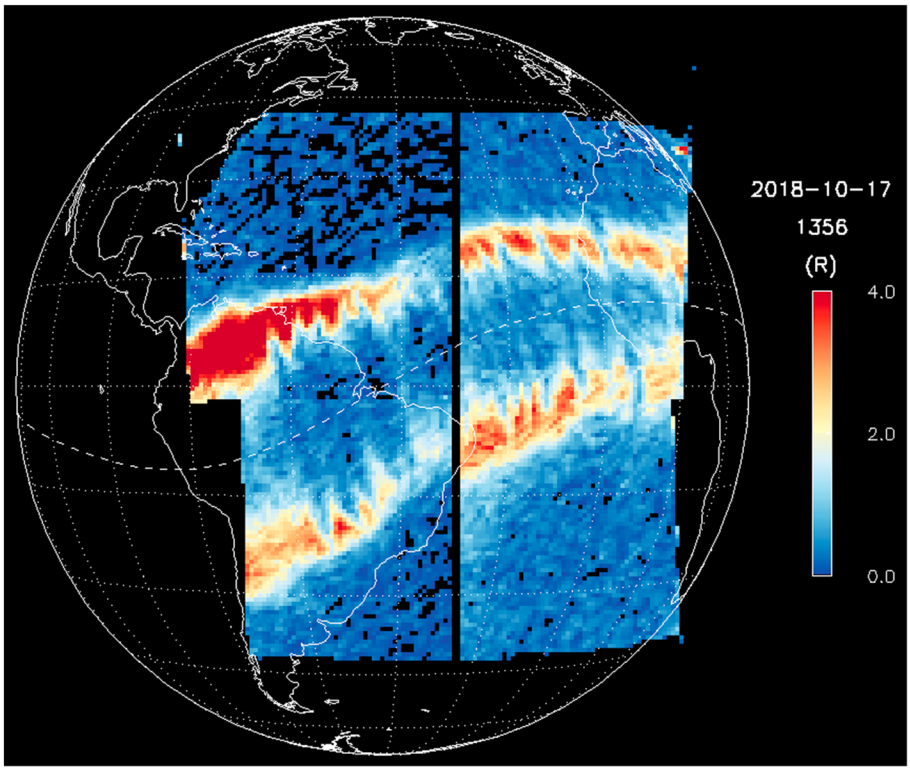

Figure 2. Image of Global-scale Observations of the Limb and Disk nighttime observations on 17 October 2018, showing the structure of the equatorial ionization anomaly, and the depletions within it. Four night mode scans, two north and two south of the equator, each of 15-min duration, are shown. The two eastern scans began at 21:10 UT, and the two western scans began at 23:55 UT. Individual scans are limited to ~30° of longitude near sunset.

time is available for repeated observations; the African region least favorable for identification of depletions, due to the off nadir viewing geometry, increasing the probability of missing some depletions. The slightly lower rates in the non-Atlantic regions is attributed to viewing conditions being less favorable. The rates near equinox are slightly higher than solstice, which is consistent with the results for the Atlantic region reported by Kil et al. (2009).

During solar maximum, previous satellite observations found the highest occurrence rates in the Atlantic sector during September–December, ~45–50% of nights, in the 1999–2002 period (Burke, Huang, et al., 2004, Burke, Gentile, et al., 2004; Comberiate & Paxton, 2010; Gentile et al., 2006). However, solar minimum occurrence rates from DMSP were much lower, similar to results from the GUVI instrument on the TIMED satellite, which found only ~5% of nights at solar minimum (Comberiate & Paxton, 2010; Gentile et al., 2006). Higher occurrence rates, 90–100% of orbits, were seen at in the CHAMP (400-km orbit) data by Stolle et al. (2008) at some longitudes during the 2001–2004 solar maximum period. Kil et al. (2009) also

Table 1
Depletion Occurrence Rates in GOLD Images

Month(s) of 2018	# of observation nights	Occurrence rates, South America (75°W to 30°W)	Occurrence rates, Atlantic (30°W to 15°W)	Occurrence rates, Africa (15°W to 15°E)
October–November	58	73%	83%	51%
December	30	54%	48%	17%

Note. GOLD = Global-scale Observations of the Limb and Disk.

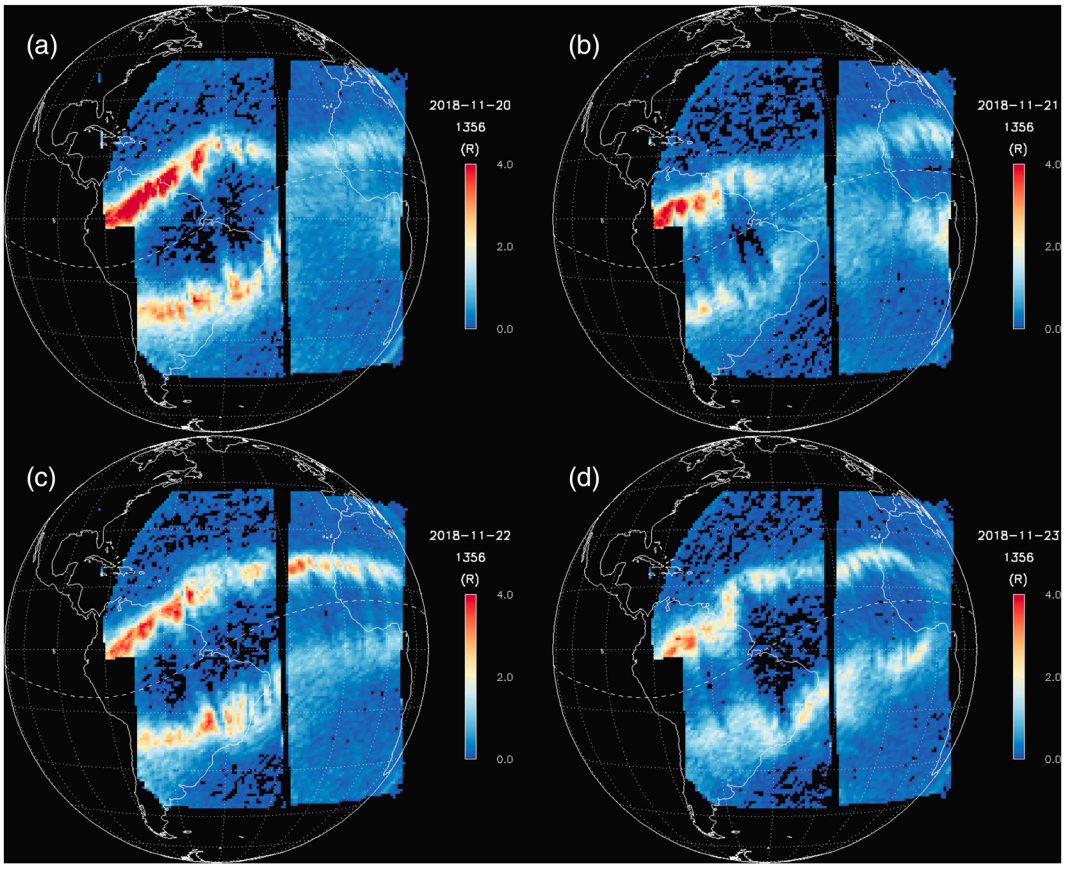

Figure 3. Quiet time variability of the equatorial ionization anomaly: (a–d) Images from four sequential nights during geomagnetically quiet conditions on 20–23 November 2018. All images are multiscan combinations, at 21:10 and 23:55 UT, as in Figure 2.

using ROCSAT and TIMED/GUVI observations near solar maximum, also found irregularities on nearly all nights. The orbit of ROCSAT (35° inclination and 600-km altitude) increases the probability detection versus the DMSP measurements. Since the occurrence rates in the DMSP data near solar maximum were a factor of 2–3 higher those near solar minimum, the ROCSAT occurrence rates are considered consistent with GOLD.

3.3. Variability of the EIA

Variability in the EIA extends beyond the depletions within the crests discussed above. Significant changes in the EIA are frequently seen even at geomagnetically quiet conditions during these solar minimum observations. Shown in Figure 3 is an example of the changes seen on four successive nights. As in Figure 2, near-sunset images have been combined. Also in Figure 3, especially in panel (b), one can see that the bubbles are curved, but the curvature reverses in observations west and east of the satellite (at 47.5°W). It is clear that the viewing geometry, combined with the curvature of the magnetic field which constrains bubbles, is a significant factor.

Some deviations in the separation of the crests are challenging to reconcile with current models of the ionosphere system. Figure 4 shows an example from 18 November 2018. The abrupt shift of the EIA to higher latitudes that occurs near 30° west longitude displaces each crest of the EIA by ~15° in latitude, to approximately twice the magnetic latitude of adjacent longitudes. The EIA persists there during four consecutive scans over a 2-hr period. Geomagnetic conditions were very quiet; the *Kp* index at the time of the observations was 1, and *Kp* for the four preceding days ranged from 1− to 1+. No unusual tropospheric weather was observed in their vicinity, either. There is a possibility that penetration electric fields are responsible for the deviation as a small, isolated, negative excursion in the interplanetary

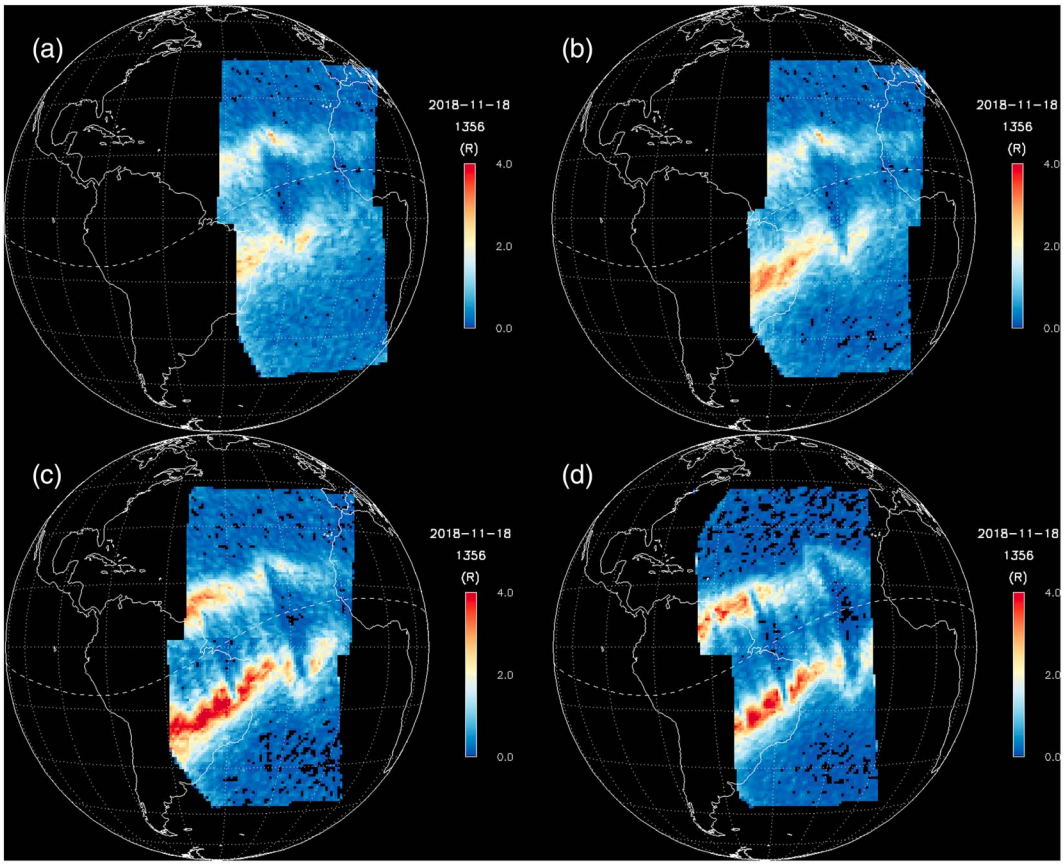

Figure 4. Latitudinal displacements of the equatorial ionization anomaly (EIA): Significant changes in the location of the EIA are observed during quiet geomagnetic conditions. This sequence shows four consecutive scan pairs on 18 November 2018, at (a) 21:40 UT, (b) 22:10 UT, (c) 22:40 UT, and (d) 23:10 UT. The displacement near the 30°W meridian occurs over only ~10° of longitude, changing the location of the EIA by up to ~15° in latitude. Each of the four images contains two 15-min scans, one in the Northern Hemisphere and one in the Southern Hemisphere, starting at 22:40 UT on 18 November 2018.

magnetic field *Bz* (~10-min duration, to −2 nT) occurred near 20:20 UT. Similar shifts occur on six nights during November 2018, or ~20% of nights. To our knowledge, these abrupt shifts have not been previously identified.

4. Conclusions

GOLD observations provide an unprecedented view of the nighttime, equatorial anomaly from western Africa to western South America. A number of features stand out. There are large variations in the morphology of the anomaly from night-to-night and also within a night, as the ~15° latitude shift in Figure 4 shows. Such abrupt shifts in the location of the EIA over limited longitudes could be responsible for some reports of broad depletions (e.g., Huang et al., 2011). On some nights, the crests weaken dramatically later in the evening; on other nights they maintain their structure throughout the observations. The separation during a night can vary greatly with longitude; sometimes, the crests appear to join. These changes are presumably caused by the upward vertical drifts associated with the PRE, suggesting that spatial and temporal variations in the PRE may be dynamic even during periods of low geomagnetic activity.

Mesoscale depletions are also a common feature in GOLD images of the anomaly. Some previous studies have suggested that the depletions (and presumable accompanying microscale phenomena) are not frequent at solar minimum.

The depletions frequently exhibit regular spacing (e.g., Figure 2). This suggests a periodic seeding mechanism. Previous in situ observations (e.g., Thampi et al., 2009) suggest that large-scale (500–700 km) wave structures may be responsible, as postulated by Hines (1960).

The phenomena described here have societal consequences (since they are associated with disruptions in communications and satellite navigation), and they illuminate frontiers in ion-neutral coupling physics. The next steps for analysis will be comparing these images with other space-based and ground-based observations, especially by Global Navigation Satellite Systems receivers and ionosondes, to identify the relationships between them. Seasonal statistics will be valuable for understanding the EIA response to atmospheric tides and will guide future attempts to describe these phenomena with numerical models. GOLD presents a new ability to image the variability of ionospheric plasma and, ultimately, to understand its causes.

Acknowledgments
The authors thank the hundreds of people who had a role in the GOLD mission, including those at CU/LASP, CPI, UCF, UCB/SSL, NASA HQ, NASA GSFC, SES, Airbus, Arianespace, ESA, CNES, CSG, and those who served on the many review panels. GOLD Level 1 data are available at http://gold.cs.ucf.edu and at the NASA Space Physics Data Facility. J. H. King and N. Papatashvilli at AdnetSystems, NASA GSFC, and CDAWeb are acknowledged for providing IMF data. R. Eastes thanks Chaosong Huang, Wenbin Wang, and Yongliang Zhang for discussions about the effects of IMF *Bz* on the EIA location. This research was supported by NASA Contract 80GSFC18C0061 to the University of Colorado. NCAR is also supported by the National Science Foundation. The Level 1C data used in this study are available at the GOLD Science Data Center (http://gold.cs.ucf.edu/search/) and at NASA's Space Physics Data Facility (https://spdf.gsfc.nasa.gov).

References

Abdu, M., & Kherani, E. A. (2011). Coupling processes in the equatorial spread F/plasma bubble irregularity development. In M. A. Abdu & D. Pancheva (Eds.), *Aeronomy of the Earth's atmosphere and ionosphere*, *IAGA Special Sopron Book Series 2* (Chap. 16, pp. 219–238). Springer Science+Business Media B. V. https://doi.org/10.1007/978-94-007-0326-1_16

Anderson, D., & Araujo-Pradere, E. A. (2010). Sudden stratospheric warming event signatures in daytime **E**×**B** drift velocities in the Peruvian and Philippine longitude sectors for January 2003 and 2004. *Journal of Geophysical Research*, *115*, A00G05. https://doi.org/10.1029/2010JA015337

Appleton, E. V. (1946). Two anomalies in the ionosphere. *Nature*, *157*(3995), 691. https://doi.org/10.1038/157691a0

Balachandran Nair, R., Balan, N., Bailey, G. J., & Rao, R. B. (1992). Spectra of the ac electric fields in the post-sunset *F*-region at the magnetic equator. *Planetary and Space Science*, *40*(5), 655–662. https://doi.org/10.1016/0032-0633(92)90006-A

Balan, N., Liu, L. B., & Le, H. J. (2018). A brief review of equatorial ionization anomaly and ionospheric irregularities. *Earth and Planetary Physics*, *2*(4), 1–19. http://doi.org/10.26464/epp2018025

Burke, W. J., Gentile, L. C., Huang, C. Y., Valladares, C. E., & Su, S. Y. (2004). Longitudinal variability of equatorial plasma bubbles observed by DMSP and ROCSAT-1. *Journal of Geophysical Research*, *109*, A12301. https://doi.org/10.1029/2004JA010583

Burke, W. J., Huang, C. Y., Gentile, L. C., & Bauer, L. (2004). Seasonal- longitudinal variability of equatorial plasma bubble occurrence. *Annales de Geophysique*, *22*, 3089–3098. SRef-ID: 1432-0576/ag/2004-22-3089

Chapagain, N. P., Taylor, M. J., & Eccles, J. V. (2011). Airglow observations and modeling of F region depletion zonal velocities over Christmas Island. *Journal of Geophysical Research*, *116*, A02301. https://doi.org/10.1029/2010JA015958

Comberiate, J., & Paxton, L. J. (2010). Global Ultraviolet Imager equatorial plasma bubble imaging and climatology, 2002–2007. *Journal of Geophysical Research*, *115*, A04305. https://doi.org/10.1029/2009JA014707 A4

Earle, G. D., & Kelley, M. C. (1987). Spectral studies of the sources of ionospheric electric fields. *Journal of Geophysical Research*, *92*(A1), 213. https://doi.org/10.1029/JA092iA01p00213

Eastes, R. W., McClintock, W. E., Burns, A. G., Anderson, D. N., Andersson, L., Codrescu, M., et al. (2017). The Global-scale Observations of the Limb and Disk (GOLD) mission. *Space Science Reviews*, *212*(1-2), 383–408. https://doi.org/10.1007/s11214-017-0392-2

Fang, T.-W., Fuller-Rowell, T., Akmaev, R., Wu, F., Wang, H., & Anderson, D. (2012). Longitudinal variation of ionospheric vertical drifts during the 2009 sudden stratospheric warming. *Journal of Geophysical Research*, *117*, A03324. https://doi.org/10.1029/2011JA017348 A3

Gentile, L. C., Burke, W. J., & Rich, F. J. (2006). A global climatology for equatorial plasma bubbles in the topside ionosphere. *Annales de Geophysique*, *24*(1), 163–172. https://doi.org/10.5194/angeo-24-163-2006

Goncharenko, L. P., Chau, J. L., Liu, H.-L., & Coster, A. J. (2010). Unexpected connections between the stratosphere and ionosphere. *Geophysical Research Letters*, *37*, L10101. https://doi.org/10.1029/2010GL043125 10

Hagan, M. E., Maute, A., Roble, R. G., Richmond, A. D., Immel, T. J., & England, S. L. (2007). The effects of deep tropical clouds on the Earth's ionosphere. *Geophysical Research Letters*, *34*, L20109. https://doi.org/10.1029/2007GL030142

Hickey, D. A., Martinis, C. R., Mendillo, M., Baumgardner, J., Wroten, J., & Milla, M. (2018). Simultaneous 6300 Å airglow and radar observations of ionospheric irregularities and dynamics at the geomagnetic equator. *Annales de Geophysique*, *36*(2), 473–487. https://doi.org/10.5194/angeo-36-473-2018

Hines, C. O. (1960). Internal atmospheric gravity waves at ionospheric heights. *Canadian Journal of Physics*, *38*(11), 1441–1481. https://doi.org/10.1139/p60-150

Huang, C.-S. (2017). The characteristics and generation mechanism of small-amplitude and large-amplitude ESF irregularities observed by the C/NOFS satellite. *Journal of Geophysical Research: Space Physics*, *122*, 8959–8973. https://doi.org/10.1002/2017JA024041

Huang, C.-S., de La Beaujardiere, O., Roddy, P. A., Hunton, D. E., Pfaff, R. F., Valladares, C. E., & Ballenthin, J. O. (2011). Evolution of equatorial ionospheric plasma bubbles and formation of broad plasma depletions measured by the C/NOFS satellite during deep solar minimum. *Journal of Geophysical Research*, *116*(A3), A03309. https://doi.org/10.1029/2010JA015982

Huba, J. D., Joyce, G., & Krall, J. (2008). Three- dimensional equatorial spread F modeling. *Geophysical Research Letters*, *35*, L10102. https://doi.org/10.1029/2008GL033509 10

Immel, T. J., England, S. L., Zhang, X., Forbes, J. M., & DeMajistre, R. (2009). Upward propagating tidal effects across the E- and F-regions of the ionosphere. *Earth, Planets and Space*, *61*(4), 505–512. https://doi.org/10.1186/BF03353167

Immel, T. J., Sagawa, E., England, S. L., Henderson, S. B., Hagan, M. E., Mende, S. B., et al. (2006). Control of equatorial ionospheric morphology by atmospheric tides. *Geophysical Research Letters*, *33*, L15108. https://doi.org/10.1029/2006GL026161

Kelley, M. C., Haerendal, G., Kappler, H., Valenzuela, A., Balsley, B. B., Carter, D. A., et al. (1976). Evidence for a Rayleigh-Taylor type instability and upwelling of depleted density regions during equatorial spread-*F*. *Geophysical Research Letters*, *3*(8), 448–450. https://doi.org/10.1029/GL003i008p00448

Kelley, M. C., Makela, J. J., de La Beaujardière, O., & Retterer, J. (2011). Convective ionospheric storms: A review. *Reviews of Geophysics*, *49*, RG2003. https://doi.org/10.1029/2010RG000340

Kil, H., Paxton, L. J., & Oh, S.-J. (2009). Global bubble distribution seen from ROCSAT-1 and its association with the evening prereversal enhancement. *Journal of Geophysical Research*, *114*, A06307. https://doi.org/10.1029/2008JA013672 A6

Liu, H., Stolle, C., Förster, M., & Watanabe, S. (2007). Solar activity dependence of the electron density at 400 km at equatorial and low latitudes observed by CHAMP. *Journal of Geophysical Research*, *112*(A11). http://doi.org/10.1029/2007JA012616

Luan, X., Wang, P., Dou, X., & Liu, Y. C.-M. (2015). Interhemispheric asymmetry of the equatorial ionization anomaly in solstices observed by COSMIC during 2007-2012. *Journal of Geophysical Research: Space Physics*, *120*, 3059–3073. https://doi.org/10.1002/2014JA020820

Lühr, H., Häusler, K., & Stolle, C. (2007). Longitudinal variation of F region electron density and thermospheric zonal wind caused by atmospheric tides. *Geophysical Research Letters*, *34*, L16102. https://doi.org/10.1029/2007GL030639 16

Makela, J. J., & Otsuka, Y. (2012). Overview of nighttime ionospheric instabilities at low- and mid-latitudes: Coupling aspects resulting in structuring at the mesoscale. *Space Science Reviews*, *168*(1-4), 419–440. https://doi.org/10.1007/s11214-011-9816-6

Makela, J. J., Vadas, S. L., Muryanto, R., Duly, T., & Crowley, G. (2010). Periodic spacing between consecutive equatorial plasma bubbles. *Geophysical Research Letters*, *37*, L14103. https://doi.org/10.1029/2010GL043968

McClintock, W. E., Eastes, R., Anderson, D. N., Andersson, L., Burns, A. G., Codrescu, M., et al. (2017). Global-scale Observations of the Limb and Disk (GOLD): Science implementation. American Geophysical Union Fall Meeting, SA31A-2561.

Retterer, J. M. (2010). Forecasting low-latitude radio scintillation with 3-D ionospheric plume models, I: plume model. *Journal of Geophysical Research*, *115*, A03306. https://doi.org/10.1029/2008JA013839 A3

Rodríguez-Zuluaga, J., Stolle, C., Yamazaki, Y., Lühr, H., Park, J., Scherliess, L., & Chau, J. L. (2019). On the balance between plasma and magnetic pressure across equatorial plasma depletions. *Journal of Geophysical Research: Space Physics*, *124*. https://doi.org/10.1029/2019JA026700

Saito, S., & Maruyama, T. (2007). Large-scale longitudinal variation in ionospheric height and equatorial spread F occurrences observed by ionosondes. *Geophysical Research Letters*, *34*, L16109. https://doi.org/10.1029/2007GL030618 16

Stolle, C., Manoj, C., Lühr, H., Maus, S., & Alken, P. (2008). Estimating the daytime Equatorial Ionization Anomaly strength from electric field proxies. *Journal of Geophysical Research*, *113*, A09310. https://doi.org/10.1029/2007JA012781

Su, S.-Y., Liu, C. H., Ho, H. H., & Chao, C. K. (2006). Distribution characteristics of topside ionospheric density irregularities: Equatorial versus midlatitude regions. *Journal of Geophysical Research*, *111*, A06305. https://doi.org/10.1029/2005JA011330

Takahashi, H., Wrasse, C. M., Otsuka, Y., Ivo, A., Gomes, V., Paulino, I., et al. (2015). Plasma bubble monitoring by TEC map and 630 nm airglow image. *Journal of Atmospheric and Terrestrial Physics*, *130-131*, 151–158. https://doi.org/10.1016/j.jastp.2015.06.003

Thampi, S. V., Yamamoto, M., Tsunoda, R. T., Otsuka, Y., Tsugawa, T., Uemoto, J., & Ishii, M. (2009). First observations of large-scale wave structure and equatorial spread F using CERTO radio beacon on the C/NOFS satellite. *Geophysical Research Letters*, *36*, L18111. https://doi.org/10.1029/2009GL039887

Tsunoda, R. T. (2006). Day-to-day variability in equatorial spread F: Is there some physics missing? *Geophysical Research Letters*, *33*, L16106. https://doi.org/10.1029/2006GL025956 16

Yamazaki, Y., & Maute, A. (2017). Sq and EEJ—A review on the daily variation of the geomagnetic field caused by ionospheric dynamo currents. *Space Science Reviews*, *206*(1-4), 299–405. https://doi.org/10.1007/s11214-016-0282-z

Zhan, W., Rodrigues, F., & Milla, M. (2018). On the genesis of postmidnight equatorial spread F: Results for the American/Peruvian sector. *Geophysical Research Letters*, *45*, 7354–7361. https://doi.org/10.1029/2018GL078822